

UC San Diego

UC San Diego Previously Published Works

Title

Cross-sectional and longitudinal multimodal structural imaging in prodromal Huntington's disease

Permalink

<https://escholarship.org/uc/item/7wr7k35t>

Journal

Movement Disorders, 31(11)

ISSN

0885-3185

Authors

Harrington, Deborah L
Long, Jeffrey D
Durgerian, Sally
[et al.](#)

Publication Date

2016-11-01

DOI

10.1002/mds.26803

Peer reviewed



Published in final edited form as:

Mov Disord. 2016 November ; 31(11): 1664–1675. doi:10.1002/mds.26803.

Cross-Sectional and Longitudinal Multimodal Structural Imaging in Prodromal Huntington's Disease

Deborah L. Harrington, PhD^{1,2}, Jeffrey D. Long, PhD³, Sally Durgerian, BS⁴, Lyla Mourany, MS⁵, Katherine Koenig, PhD⁶, Aaron Bonner-Jackson, PhD⁷, Jane S. Paulsen, PhD³, and Stephen M. Rao, PhD⁵ for the PREDICT-HD investigators of the Huntington Study Group

¹Department of Radiology, University of California, San Diego, La Jolla, CA, USA

²Research Service, VA San Diego Healthcare System, San Diego, CA, USA

³Carver College of Medicine, The University of Iowa, Iowa City, IA, USA

⁴Department of Neurology, Medical College of Wisconsin, Milwaukee, WI, USA

⁵Schey Center for Cognitive Neuroimaging, Neurological Institute, Cleveland Clinic, Cleveland, OH, USA

⁶Imaging Sciences, Imaging Institute, Cleveland Clinic, Cleveland, OH, USA

⁷Lou Ruvo Center for Brain Health, Neurological Institute, Cleveland Clinic, OH, USA

Abstract

Objectives—Diffusivity in white-matter tracts is abnormal throughout the brain in cross-sectional studies of prodromal Huntington's disease. To date, longitudinal changes have not been observed. The present study investigated cross-sectional and longitudinal changes in white-matter diffusivity in relationship to the phase of prodromal Huntington's progression, and compared them with changes in brain volumes and clinical variables that track disease progression.

Methods—Diffusion MRI profiles were studied over two years in 37 gene-negative controls and 64 prodromal Huntington's disease participants in varied phases of disease progression. To estimate the relative importance of diffusivity metrics in the prodromal phase, group effects were rank ordered relative to those obtained from analyses of brain volumes, motor, cognitive and sensory variables.

Results—First, at baseline diffusivity was abnormal throughout all tracts, especially as individuals approached a manifest Huntington's disease diagnosis. Baseline diffusivity metrics in six tracts and basal ganglia volumes best distinguished amongst the groups. Second, group differences in longitudinal change in diffusivity were localized to the superior fronto-occipital fasciculus, most prominently in individuals closer to a diagnosis. Group differences were also observed in longitudinal changes of most brain volumes, but not clinical variables. Lastly, increases in motor symptoms across time were associated with greater changes in the superior

fronto-occipital fasciculus diffusivity and corpus callosum, cerebrospinal fluid, and lateral ventricle volumes.

Conclusions—These novel findings provide new insights into changes within two years in different facets of brain structure and their clinical relevance to changes in symptomatology that is decisive for a manifest Huntington’s diagnosis.

Keywords

Huntington’s disease; diffusion tensor imaging; brain volume; motor symptoms; cognition

Introduction

Huntington’s disease (HD) is a fatal neurodegenerative disorder characterized by a triad of motor, cognitive and psychiatric disturbances. HD is caused by a cytosine-adenine-guanine (CAG) repeat expansion in the huntingtin (HTT) gene. HTT is expressed throughout the brain and body, but medium spiny neurons of the striatum are selectively targeted early in the prodromal phase (prHD), followed by less prominent cortical grey (GM) and white (WM) matter loss.¹⁻⁴ In anticipation of treatments designed to prevent or slow the development of signs and symptoms, outcomes for clinical trials are needed that are sensitive to changes in the prodromal phase when interventions may be most effective. Although motor and cognitive variables track disease progression and predict time to diagnosis,¹⁻³ striatal volumes are particularly robust markers.²⁻⁵ However, striatal volume might not be the most sensitive marker for all interventions, which can differ in their mechanisms of action or the time window to produce an effect. It is therefore important to study structural markers of disease progression throughout the brain.

WM volume loss also tracks disease progression in prHD,^{3,6-8} suggesting pathological changes in the structural connectivity of corticostriatal and cortico-cortical pathways. In this regard, diffusion MRI (dMRI) is of keen interest as it measures local microstructural characteristics of water diffusion in tissues, potentially elucidating pathological processes associated with neurodegeneration in WM tracts. Cross-sectional dMRI studies of prHD report WM pathology throughout anterior and posterior tracts,^{9,10} tracts innervating prefrontal cortex,¹¹⁻¹³ frontostriatal and sensorimotor tracts,¹⁴⁻¹⁶ and the corpus callosum.¹⁶⁻²⁰ Although WM pathology correlates with disease burden in some studies,^{9,11,12,14} longitudinal studies are needed to chart the course of disease progression. However, most longitudinal dMRI studies of prHD have not found abnormal 12 to 30-month changes in diffusivity profiles of whole-brain WM,²¹ centers of WM tracts,²² or the striatum,^{4,5,21} although the latter result may relate to limitations of the tensor model in GM. Longitudinal dMRI findings contrast with 12 to 24-month striatal, GM, and WM volume loss in prHD,^{4-6,8,23} suggesting volumetric measures may be more sensitive to longitudinal changes. This issue requires further examination owing to the small prHD samples in longitudinal dMRI studies (i.e., 22 to 40) and the limited number of investigations examining diffusivity profiles within WM tracts.²²

The present study builds upon previous results by characterizing two-year changes in diffusivity profiles of 64 prHD individuals in different phases of disease progression to

evaluate its relationship to the evolution of WM pathology. Differences amongst groups at baseline were also tested to provide a context for the longitudinal results. To estimate the relative sensitivity of dMRI and other variables known to track disease progression, measures of brain volume, cognition, and motor symptoms were also obtained. The results are expected to inform the ongoing refinement of dMRI outcomes and selection of potential targets for clinical interventions. Relationships between longitudinal changes in MRI and behavioral variables are also reported, which may have value in choosing outcomes associated with clinically meaningful endpoints.

Methods

Participants

Participants underwent baseline, 12- and 24-month assessments. Data were collected at the Cleveland Clinic and the University of Iowa as part of the larger PREDICT-HD study.^{2,24} Ethics committees at both sites approved the study. Participants completed genetic testing for the CAG expansion. Certified examiners administered the Unified Huntington's Disease Rating Scale (UHDRS) Motor Assessment. Examiners rated their Diagnostic Confidence Level (DCL) that a participant's motor signs were indicative of HD; volunteers were excluded with a DCL of 4 (99% confidence of unequivocal signs of HD).

The sample at the baseline visit consisted of 64 gene-positive prHD individuals and 37 gene-negative controls with a family history of HD. Exclusion criteria included clinical evidence of unstable medical/psychiatric illness, alcohol/drug abuse within the past year, learning/developmental disability requiring special education, history of another neurological condition, inability to undergo MRI scanning, and use of prescription antipsychotic medications within the past six months or phenothiazine-derivative antiemetic medications more than three times per month. The prHD participants were stratified into Low (n=19), Medium (n=28), and High (n=17) baseline progression groups based on the CAG-Age Product, a widely used index of disease burden computed as $CAP = [(age \text{ at study entry}) \times (CAG \text{ repeats} - 33.66)]$.^{25,26} Using this stratification, estimated time to motor diagnosis (DCL = 4) is > 12.78 years, 12.78 to 7.59 years, and < 7.59 years for Low, Medium, and High groups, respectively.

Clinical assessments

At each visit, tests of executive, sensory, and motor functions that track disease progression in prHD were administered including: 1) Stroop Color and Word Test (color naming, word reading, and interference; total correct in 45s); 2) Symbol Digit Modalities Task (total correct in 90 s); 3) Trail Making Test (Parts A and B; time to complete), 4) University of Pennsylvania Smell Identification Test (UPSIT) (percent correct)³, and 5) UHDRS total motor score (TMS; 31 items) and chorea (7 items), oculomotor (6 items), bradykinesia (11 items), rigidity (2 items), and dystonia (5 items) scores.²⁷

Neuroimaging protocol

Both sites used Siemens TIM Trio 3T MRI scanners with a 12-channel receive-only head array. Frequent quality assurance scans were performed at each institution to ensure that data

were free of scanner artifacts and comparable between sites in image quality and signal-to-noise. We acquired whole brain T1-weighted inversion recovery turboflash (MPRAGE) images [166 axial slices; thickness=1 mm; field-of-view (FOV) = 256×240 mm²; inversion time (TI)/echo time (TE)/repetition time (TR)/flip angle = 900/3.04/2530 ms/10°; matrix = 256×240; receiver bandwidth (BW) = 220 kHz] and high angular resolution diffusion images (twice-refocused spin echo diffusion weighting, single-shot 2D echo planar imaging readout, 2mm isotropic resolution, 256mm x 256mm FOV, 128 x 128 matrix, 50 2mm thick slices, TE = 92msec, TR = 7600 msec, partial Fourier factor 5/8, readout bandwidth 1562 Hz/Pixel, 71 diffusion-weighted volumes with b = 1000 sec/mm², 8 b = 0 volumes, NEX = 3).^{28,29}

Anatomical MRI analysis

MRI scans were analyzed for bilateral regional cortical and subcortical volumes, since hemispheric asymmetries have not been noted in prHD. Brain volumes were derived using the FreeSurfer 5.3 longitudinal analysis pipeline, which demonstrates good test-retest reliability across scanners and sites.³⁰ Volumetric measures were adjusted for total intracranial volume [(volume/intracranial volume) x 100]. Nine structures were studied that exhibit longitudinal volume loss in prHD including the putamen, caudate, globus pallidus, accumbens, corpus callosum, cortical GM and WM, cerebrospinal fluid (CSF), and lateral ventricles.^{3,6,7,31,32}

dMRI analysis

After motion and eddy-current correction,³³ data were fit on a voxel-by-voxel basis to the diffusion tensor model, accounting for noise floor bias with a maximum likelihood estimation approach. Measures of tissue microstructure [fractional anisotropy (FA), mean diffusivity (MD), axial diffusivity (AD), radial diffusivity (RD)] were calculated from the diffusion tensor in each voxel by matrix diagonalization with in-house software.³⁴

Data were then processed using Tract-Based Spatial Statistics (TBSS) preprocessing functions in FSL 5.0.8 (<http://www.fmrib.ox.ac.uk/fsl/tbss/index.html>).³⁵ FA images were nonlinearly registered to FMRIB58_FA and then to a study-specific FA template in MNI space. Nonlinear transforms were also applied to the diffusivity volumes. Regions of interest (ROIs) were created using the JHU-ICBM-labels WM atlas, which contains WM tracts hand-segmented on an average probabilistic tensor map of 81 healthy subjects.³⁶ Of the 48 atlas ROIs, 32 left and right hemisphere tracts and three midline tracts were covered by dMRI scans for all subjects. In preliminary analyses, group differences in longitudinal change were not related to the hemisphere of a tract. To reduce multiple analyses, homologous hemispheric tracts were combined into a single bilateral ROI by multiplying diffusion metrics of a tract by each hemisphere volume, then summing the products and dividing by the total volume. This produced 19 ROIs per diffusion metric.

Statistical analysis

All measures were analyzed in R 3.2.2 (<https://www.R-project.org/>) using linear mixed effects regression (LMER).³⁷ Orthogonal polynomial contrasts were used to test group effects (Negative, Low, Medium, High). The model included time (years), wherein 0 = study

entry, and baseline covariates: [(age + age²) * time + sex + education + study site]. Subject-specific random effects were specified for baseline (intercept) and time (slope). Of primary interest was the group by time interaction, representing group differences in the rate of change over time for an outcome. An omnibus approach for testing group differences was used, wherein both intercept and slope differences were simultaneously tested. Omnibus testing was conducted by comparing 1) a reduced model omitting group and including covariates and the time effect and 2) a full model that added the main effect of group at baseline (intercept) and the group by time interaction. LMER models were estimated using maximum likelihood methods, which produce unbiased estimates under the assumption that the missing data mechanism is ignorable. The likelihood ratio test (LRT) was used for the omnibus test. Owing to the large number of outcome variables, the false discovery rate (FDR) adjustment was applied separately to each domain of variables (19 ROI for each diffusion metric; 9 brain volumes; 6 motor variables; 7 cognitive/sensory variables). When a variable showed a significant LRT of the full model ($q < 0.05$), general linear hypothesis (GLH) tests were performed to test for the specific effects of group, both baseline differences and the group by time interaction (i.e., slope differences). Because these were follow-up analyses, we considered the FDR adjustment for the LRT to be adequate type I error rate protection (i.e., unadjusted p-values for GLH tests).

Simple regression was used to investigate relationships between: 1) disease burden (baseline CAP) and MRI variables that showed significant group by time interactions (GLH tests); 2) dMRI variables and brain volumes that showed significant group by time interactions (GLH tests), and 3) annualized rates of change in MRI variables showing a significant group by time interaction (GLH tests) and rates of change in selected motor, cognitive, and sensory variables (irrespective of whether group by time differences were significant). For these analyses, subject-specific slopes for prHD participants were computed based on the fitted LMER model. Then slopes for variables of interest were correlated (FDR adjusted) controlling for nuisance variables.

Results

Participants

At baseline, the Low group was younger than the other groups and the Medium group was younger than the High group (Table 1). Education and sex were well balanced amongst groups. The High group showed more motor signs than other groups and performed more poorly than the Negative group on the Stroop Word and the Trail Making Test Part B. For the second and third visits, there was data loss owing to attrition or exclusion of poor quality dMRI data (e.g., motion artifact): Negative: n=35, 25; Low: n=17, 11; Medium: n=24, 23; and High: n=15, 11 for 12- and 24-month visits, respectively. Data loss was greater in the prHD (12%) than the Negative (5%) group at the 12-month, but not the 24-month visit (Negative = 32%; prHD=30%). There was no difference in data loss amongst prHD groups at the 12-month visit (11% to 14%); at the 24-month visit less data was lost in the Medium (18%) than the Low (42%) and High (35%) groups. These results suggest that disease burden was not a factor in attrition or poor quality dMRI data. The groups did not differ in

the number of years between the baseline and last study visit [$F=0.45$, $p=0.72$; mean (SE): Negative 1.68 (0.60); Low 1.56 (0.77); Medium 1.71 (0.75); High 1.62 (0.64)].

LMER tests of the full model

Table A1 (Appendix) summarizes the results from the LMER of the dMRI variables. The full model had superior fit for MD and/or RD in all tracts (i.e., significant LRT), suggesting aberrant WM throughout the brain in prHD at baseline and/or longitudinally, especially perpendicular to the axon (RD). Omnibus tests of the full model for FA and AD were significant in 58% and 47% of the tracts, respectively. Thus, aberrant changes parallel to the axonal tract (AD) were confined to specific tracts at baseline and/or longitudinally. Table A2 (Appendix) shows that the full model had the best fit for all brain volumes, except cortical GM. Significant LRTs of the full model were found for some motor (TMS, chorea, bradykinesia) and cognitive (Stroop Color Naming, Stroop Word Reading) measures. Sources of the significant omnibus tests of the full model are detailed in Tables 2 and 3.

GLH tests for cross-sectional group differences

Baseline group differences in various diffusion metrics were observed for all WM tracts (see JHU-ICBM atlas).³⁶ As the phase of prodromal disease progressed, MD and/or RD gradually increased in all tracts (Table 2). Decreases in FA and increases in AD as phase of disease progressed were found in 58% and 47% of the tracts, respectively. As for brain volumes, basal ganglia volumes decreased and CSF and lateral ventricle volumes increased with disease progression group (Table 2). Motor symptoms (TMS, chorea, and bradykinesia) increased and Stroop Word reading test performance worsened with disease progression.

The descending rank of the chi-square statistics is shown in the last column. The top 15 ranked variables that most robustly differentiated amongst the groups at baseline included putamen (#1), caudate (#4), and pallidum (#10) volumes and diffusivity metrics in six tracts, namely the external capsule (MD #2; RD #3; AD #7), fornix-stria terminalis (RD #5; MD #6), posterior thalamic radiations (AD #8; MD #9), cingulum (hippocampal projection; MD #11; AD #15), body of the corpus callosum (FA #12; RD #13), and anterior limb of the internal capsule (RD#14). Other volumetric, motor, and cognitive variables were not ranked highly.

GLH tests for longitudinal group differences

Significant group differences in the rate of change in WM diffusivity were found only for MD in the superior fronto-occipital fasciculus (SFOF). Annualized linear increases in MD were notable mostly in the High group (Table 3; Figure 1). Significant group differences in longitudinal change were also found for all regional brain volumes, except the nucleus accumbens (Table 3; Figure 1). Linear decreases in caudate, putamen, corpus callosum and cortical WM were prominent in the High group as were increases in CSF and lateral ventricle volumes. No group differences were found in annualized rates of change for motor and cognitive variables.

The rank ordering of the chi-square statistics (Table 3) indicated that group differences were best distinguished by linear changes in the basal ganglia (#1, 2), lateral ventricles (#3),

corpus callosum (#4), and cortical WM (#5) volumes, followed by SFOF MD (#6) and CSF volume (#7).

Relationships between longitudinal change in MRI and clinical variables

Simple regression, adjusting for age and number of years between the baseline and the final MRI visit, was used to characterize relationships between disease burden and annualized changes in the MRI variables that showed significant group by time interactions. Increases in baseline CAP significantly correlated with longitudinal increases in SFOF MD ($r_{xy,z} = 0.35$, $q < 0.05$) and lateral ventricle volume ($r_{xy,z} = 0.34$, $q < 0.05$) and decreases in caudate volume ($r_{xy,z} = -0.463$, $q < 0.01$). Baseline CAP was not associated with changes in corpus callosum, cortical WM, CSF or putamen volume.

To characterize associations between rates of change in SFOF MD and brain volumes that exhibited significant group by time interactions, simple regression adjusting for age was used to correlate subject slopes in the prHD group. Longitudinal increases in SFOF MD strongly correlated with increases in lateral ventricle volume ($r_{xy,z} = 0.76$, $q < .001$) and moderately correlated with decreases in caudate ($r_{xy,z} = -0.45$, $q < .01$) and putamen ($r_{xy,z} = -0.31$, $q < .05$) volume. Changes in SFOF MD were not associated with changes in corpus callosum, cortical WM, or CSF volume.

Next simple regression was then used to examine the relationship between the subject slopes of the seven MRI variables that exhibited significant group by time interactions and slopes of the TMS, Stroop Word, Symbol Digit Test, Trails Part B, and UPSIT. Adjustment variables were age, CAP score, and number of years between the baseline and final MRI visit. P-values were FDR adjusted for each set of correlations between a clinical measure and the seven MRI variables. Annualized increases in the TMS (worsening) were significantly correlated with increases in CSF and lateral ventricle volume and decreases in corpus callosum volume (Figure 2). Linear increases in the TMS also correlated with increases in SFOF MD, although only a trend for significance remained after FDR adjustment ($p = 0.03$; $q = 0.055$). Annualized changes in the TMS were not associated with changes in caudate, putamen, or cortical WM volume. No significant correlations were found between slopes of the cognitive/sensory measures and slopes of the MRI variables.

Discussion

The present study investigated cross-sectional and longitudinal changes in WM diffusivity in prHD. We found abnormal diffusivity at baseline throughout all WM tracts, especially as individuals neared a motor diagnosis. A new finding was that diffusivity in six tracts best distinguished amongst the groups at baseline, along with striatal volumes. This finding builds upon past cross-sectional studies by demonstrating that aberrant WM diffusion in specific tracts characterizes phases of prHD progression as well or better than some widely-studied volumetric markers. We also found for the first time that aberrant longitudinal change in WM diffusivity was localized to the SFOF, most prominently in the High group. Longitudinal changes in most brain volumes, but not clinical variables, also differed amongst the groups. Importantly, increases in motor symptoms over time correlated with greater changes in SFOF MD and corpus callosum, CSF, and lateral ventricle volumes.

These results provide new insights into annual changes in different facets of brain structure and their relevance to a worsening in symptomatology that is decisive for a manifest motor diagnosis.

Cross-sectional changes in brain structure

Our cross-sectional results build upon previous studies by showing that as the phase of prHD progresses, MD is increased in nearly all fiber tracts owing to increased RD, which has been linked to demyelination.³⁸ Indeed, increased RD is observed in prHD throughout frontal and posterior tracts^{9,11,12,14} and corpus callosum.^{18,19} These findings are compatible with increased densities of oligodendrocytes in the prodromal phase,³⁹ which regulate axonal myelination production and repair. However, AD was also increased in 45% of the tracts, and was one of the top-ranked metrics that distinguished amongst groups at baseline in the external capsule, cingulum, and posterior thalamic radiations. Using different analytic approaches, two studies also found more localized increases in both AD and RD as individuals neared a diagnosis.^{9,12} Though pathological processes that cause changes in AD and RD are not understood, they often occur in close proximity and may signify greater early cell loss and gliosis than RD changes by themselves.⁴⁰

A new finding was that diffusivity metrics in six tracts and basal ganglia volumes comprised the top-ranked variables that best distinguished amongst the groups. Though putamen volume was ranked first,⁴¹ diffusivity in cholinergic projections from the basal forebrain to the cerebral cortex, namely the external capsule (MD/RD), were ranked second and third, followed by caudate volume. AD in the external capsule and diffusivity in limbic system pathways linking emotion to cognition (fornix and stria terminalis; RD/MD) and projections connecting occipital, temporal and parietal cortices (posterior thalamic radiation; AD/MD) were all ranked higher than pallidum volume. The remaining top-ranked variables included diffusivity metrics in association fibers connecting temporal and frontal lobes (cingulum), interhemispheric connections (corpus callosum), and projections connecting cortex with basal ganglia (anterior limb of internal capsule). Altered diffusivity in cortical-subcortical and cortical-cortical tracts, particularly in individuals near diagnosis or in early HD, may affect cognitive and emotional processing.^{1,3,42,43} Indeed, in cross-sectional studies of large prHD samples (146 participants), poorer executive functioning in prHD is associated with more aberrant diffusivity in frontal and frontostriatal WM tracts.¹² None of the clinical variables were ranked near the top, similar to a 15-month longitudinal study of manifest HD,⁴⁴ suggesting that dMRI metrics and brain volumes are better indicators of disease progression at baseline.

Longitudinal changes in brain structure

We revealed that longitudinal increases in MD of the SFOF were prominent as individuals approached a motor diagnosis and correlated with disease burden. Past studies of prHD have not uncovered significant 18- to 24-month longitudinal changes in WM using histogram analyses of the entire brain²¹ or skeleton-based analyses of central WM fibers.²² Reasons for the discrepancies are unknown, but may relate to different analytic approaches and/or small prHD samples (i.e., 22 to 28). Consistent with other studies,^{3,6,31} we also observed group differences in longitudinal change for most volumetric (striatum, corpus callosum, cortical

WM, CSF, and lateral ventricles), but not clinical variables. The latter finding agrees with a multisite study of prHD reporting no 24-month changes in clinical variables,⁶ except the TMS for which we did not find longitudinal group differences.

Changes in SFOF diffusivity appeared partially independent of changes in brain volumes, as they were only moderately associated with changes in striatal volume, the most robust marker of disease progression in prHD.^{3,6} The SFOF connects the frontal lobe with superior parietal and superior-middle occipital cortices⁴⁵, which comprise the dorsal visual stream. This network mediates higher-level motor functions and visuospatial processing used to prepare and guide movements.⁴⁶ Indeed, cognitive-motor control declines in prHD.^{47,48} SFOF architecture is compatible with the trend for a relationship between rates of change in SFOF MD and change in the TMS, which probes for oculomotor control and higher motor functions (e.g., hand pronation/supination, sequencing, tandem walking). This relationship was independent of disease burden, as were associations between changes in the TMS and changes in CSF, lateral ventricle and corpus callosum volume, the latter for which atrophy disrupts interhemispheric interactions essential for controlling movement.⁴⁹ In contrast, change in SFOF MD was not related to changes in cognitive measures, which instead correlate with prefrontal and frontostriatal WM diffusivity in cross-sectional studies of prHD.^{11,12}

Conclusions

Longitudinal changes in diffusivity were uncovered within a single tract (SFOF), the clinical relevance of which was supported by its association with baseline progression group and changes in motor symptomatology critical for a manifest motor diagnosis. These results are preliminary and require replication in a larger prHD cohort, which may also reveal longitudinal changes in other WM tracts. In addition, our cross-sectional findings revealed prominent diffusivity abnormalities within certain tracts, most of which show 15-month changes in early HD.⁵⁰ This may suggest that longer time windows are needed to better characterize WM progression in prHD. To refine future measures of aberrant WM, it will also be important to investigate different analytic approaches, including graph theory, wherein two-year changes in local network interactions of paracentral and medial prefrontal cortices were recently reported in prHD.⁵¹

Supplementary Material

Refer to Web version on PubMed Central for supplementary material.

Acknowledgments

Funding This work was supported by the National Institutes of Health, National Institute of Neurological Disorders and Stroke (5R01NS040068, 1U01NS082083, 5R01NS054893) and the CHDI Foundation (A-5008). DLH was partially supported by a grant from the Department of Veterans Affairs (CX000146).

The authors would like to thank The University of Iowa Huntington Disease Society Center of Excellence, the University of Iowa HD Research Group and Cleveland Clinic PREDICT-HD sites. We also thank the study participants, the National Research Roster for Huntington Disease Patients and Families, the Huntington's Disease Society of America, and the Huntington Study Group. We acknowledge the assistance of Mark J. Lowe, Ken E. Sakaie, Hans J. Johnson, Vincent A. Magnotta, and Jeremy H. Bockholt.

Full financial disclosure for the previous 12 months

Deborah L Harrington	
Stock Ownership in medically-related fields: None	Intellectual Property Rights: None
Consultancies: None	Expert Testimony: None
Advisory Boards: None	Employment: VA San Diego Healthcare System; University of California, San Diego
Partnerships: None	Contracts: None
Honoraria: None	Royalties: None
Grants: U.S. Department of Veterans Affairs (CX00146); NIH/NINDS U01NS082083	Other

Jeffrey D Long	
Stock Ownership in medically-related fields: None	Intellectual Property Rights: None
Consultancies: NeuroPhage LLC; Roche Pharma; Azevan Pharmaceuticals Inc	Expert Testimony: None
Advisory Boards: None	Employment: University of Iowa
Partnerships: None	Contracts: None
Honoraria: None	Royalties: None
Grants: CHDI; Michael J. Fox Foundation; NIH/NINDS 5R01NS040068, 5R01NS054893	Other

Sally Durgerian	
Stock Ownership in medically-related fields: None	Intellectual Property Rights: None
Consultancies: None	Expert Testimony: None
Advisory Boards: None	Employment: Medical College of Wisconsin
Partnerships: None	Contracts: None
Honoraria: None	Royalties: None
Grants: NIH/NINDS 1U01NS082083, 5R01NS054893	Other

Lyla Mourany	
Stock Ownership in medically-related fields: None	Intellectual Property Rights: None
Consultancies: None	Expert Testimony: None
Advisory Boards: None	Employment: Cleveland Clinic
Partnerships: None	Contracts: None
Honoraria: None	Royalties: None
Grants: None.	Other

Katherine Koenig	
Stock Ownership in medically-related fields: None	Intellectual Property Rights: None
Consultancies: None	Expert Testimony: None
Advisory Boards: None	Employment: Cleveland Clinic
Partnerships: None	Contracts: None
Honoraria: None	Royalties: None

Katherine Koenig	
Grants: : NIH/NINDS U01 NS082083; National Multiple Sclerosis Society RG4931A1; The Alana USA Foundation; The Eleanor and Kelvin Smith Foundation	Other

Aaron Bonner-Jackson	
Stock Ownership in medically-related fields: None	Intellectual Property Rights: None
Consultancies: None	Expert Testimony: None
Advisory Boards: None	Employment: Cleveland Clinic
Partnerships: None	Contracts: None
Honoraria: None	Royalties: None
Grants: None	Other

Jane S. Paulsen	
Stock Ownership in medically-related fields: None	Intellectual Property Rights: None
Consultancies: None	Expert Testimony: None
Advisory Boards: None	Employment: University of Iowa
Partnerships: None	Contracts: None
Honoraria: None	Royalties: None
Grants: NIH/NINDS 5R01NS040068, 5R01NS054893	Other

Stephen M. Rao	
Stock Ownership in medically-related fields: None	Intellectual Property Rights: None
Consultancies: None	Expert Testimony: None
Advisory Boards: None	Employment: Cleveland Clinic
Partnerships: None	Contracts: None
Honoraria: Biogen, International Neuropsychological Society, American Psychological Association	Royalties: Cleveland Clinic
Grants: NIH/NINDS 1U01NS082083; R01AG022304, R01 CA175100; National MS Society RG4931A1/1; Biogen BIOG1508S	Other

Author Roles

DLH contributed to the project design, statistical analysis, interpretation of the data, and drafted the manuscript. JDL directed the statistical analytic approaches and contributed to the review of the manuscript. SD conducted the diffusion tensor imaging and statistical analyses and reviewed the manuscript. LM contributed to data collection, processing of volumetric MRI data, and review of the manuscript. KK contributed to the post-processing of the diffusion tensor imaging data. ABJ contributed to the review of the manuscript. JSP contributed to the conceptualization of the study, project design and review of the manuscript; she is the principal investigator of the PREDICT-HD study and fMRI grants supporting this project. SMR contributed to the conceptualization of the study, project design, interpretation of the data, and review of the manuscript; he is the principal investigator of the primary NIH award supporting this project.

References

1. Harrington DL, Smith MM, Zhang Y, Carlozzi NE, Paulsen JS. Cognitive domains that predict time to diagnosis in prodromal Huntington disease. *J Neurol Neurosurg Psychiatry*. 2012; 83(6):612–619. [PubMed: 22451099]
2. Paulsen JS, Long JD, Ross CA, et al. Prediction of manifest Huntington's disease with clinical and imaging measures: a prospective observational study. *Lancet Neurol*. 2014; 13(12):1193–1201. [PubMed: 25453459]
3. Paulsen JS, Long JD, Johnson HJ, et al. Clinical and Biomarker Changes in Premanifest Huntington Disease Show Trial Feasibility: A Decade of the PREDICT-HD Study. *Front Aging Neurosci*. 2014; 6:78. [PubMed: 24795630]
4. Dominguez DJ, Egan GF, Gray MA, et al. Multi-modal neuroimaging in premanifest and early Huntington's disease: 18 month longitudinal data from the IMAGE-HD study. *PLoS ONE*. 2013; 8(9):e74131. [PubMed: 24066104]
5. Dominguez DJ, Stout JC, Poudel G, et al. Multimodal imaging biomarkers in premanifest and early Huntington's disease: 30-month IMAGE-HD data. *Br J Psychiatry*. 2015
6. Tabrizi SJ, Reilmann R, Roos RA, et al. Potential endpoints for clinical trials in premanifest and early Huntington's disease in the TRACK-HD study: analysis of 24 month observational data. *Lancet Neurol*. 2012; 11(1):42–53. [PubMed: 22137354]
7. Tabrizi SJ, Scahill RI, Owen G, et al. Predictors of phenotypic progression and disease onset in premanifest and early-stage Huntington's disease in the TRACK-HD study: analysis of 36-month observational data. *Lancet Neurol*. 2013; 12(7):637–649. [PubMed: 23664844]
8. Aylward EH, Nopoulos PC, Ross CA, et al. Longitudinal change in regional brain volumes in prodromal Huntington disease. *J Neurol Neurosurg Psychiatry*. 2011; 82(4):405–410. [PubMed: 20884680]
9. Stoffers D, Sheldon S, Kuperman JM, Goldstein J, Corey-Bloom J, Aron AR. Contrasting gray and white matter changes in preclinical Huntington disease: an MRI study. *Neurology*. 2010; 74(15):1208–1216. [PubMed: 20385893]
10. Faria AV, Ratnanather JT, Tward DJ, et al. Linking white matter and deep gray matter alterations in premanifest Huntington disease. *Neuroimage Clin*. 2016; 11:450–460. [PubMed: 27104139]
11. Matsui JT, Vaidya JG, Johnson HJ, et al. Diffusion weighted imaging of prefrontal cortex in prodromal Huntington's disease. *Hum Brain Mapp*. 2014; 35(4):1562–1573. [PubMed: 23568433]
12. Matsui JT, Vaidya JG, Wassermann D, et al. Prefrontal cortex white matter tracts in prodromal Huntington disease. *Hum Brain Mapp*. 2015; 36(10):3717–3732. [PubMed: 26179962]
13. Phillips O, Squitieri F, Sanchez-Castaneda C, et al. Deep white matter in Huntington's disease. *PLoS ONE*. 2014; 9(10):e109676. [PubMed: 25340651]
14. Poudel GR, Stout JC, Dominguez DJ, et al. White matter connectivity reflects clinical and cognitive status in Huntington's disease. *Neurobiol Dis*. 2014; 65:180–187. [PubMed: 24480090]
15. Kloppel S, Draganski B, Golding CV, et al. White matter connections reflect changes in voluntary-guided saccades in pre-symptomatic Huntington's disease. *Brain*. 2008; 131(Pt 1):196–204. [PubMed: 18056161]
16. Dumas EM, van den Bogaard SJ, Ruber ME, et al. Early changes in white matter pathways of the sensorimotor cortex in premanifest Huntington's disease. *Hum Brain Mapp*. 2012; 33(1):203–212. [PubMed: 21264990]
17. Di PM, Luders E, Cherubini A, et al. Multimodal MRI analysis of the corpus callosum reveals white matter differences in presymptomatic and early Huntington's disease. *Cereb Cortex*. 2012; 22(12):2858–2866. [PubMed: 22223853]
18. Rosas HD, Lee SY, Bender AC, et al. Altered white matter microstructure in the corpus callosum in Huntington's disease: implications for cortical "disconnection". *Neuroimage*. 2010; 49(4):2995–3004. [PubMed: 19850138]
19. Phillips O, Sanchez-Castaneda C, Elifani F, et al. Tractography of the corpus callosum in Huntington's disease. *PLoS ONE*. 2013; 8(9):e73280. [PubMed: 24019913]

20. Rosas HD, Tuch DS, Hevelone ND, et al. Diffusion tensor imaging in presymptomatic and early Huntington's disease: Selective white matter pathology and its relationship to clinical measures. *Mov Disord.* 2006; 21(9):1317–1325. [PubMed: 16755582]
21. Odish OF, Leemans A, Reijntjes RH, et al. Microstructural brain abnormalities in Huntington's disease: A two-year follow-up. *Hum Brain Mapp.* 2015; 36(6):2061–2074. [PubMed: 25644819]
22. Poudel GR, Stout JC, Dominguez DJ, et al. Longitudinal change in white matter microstructure in Huntington's disease: The IMAGE-HD study. *Neurobiol Dis.* 2015; 74:406–412. [PubMed: 25497085]
23. Tabrizi SJ, Scahill RI, Durr A, et al. Biological and clinical changes in premanifest and early stage Huntington's disease in the TRACK-HD study: the 12-month longitudinal analysis. *Lancet Neurol.* 2011; 10(1):31–42. [PubMed: 21130037]
24. Paulsen JS, Langbehn DR, Stout JC, et al. Detection of Huntington's disease decades before diagnosis: the Predict-HD study. *J Neurol Neurosurg Psychiatry.* 2008; 79(8):874–880. [PubMed: 18096682]
25. Zhang Y, Long JD, Mills JA, Warner JH, Lu W, Paulsen JS. Indexing disease progression at study entry with individuals at-risk for Huntington disease. *Am J Med Genet B Neuropsychiatr Genet.* 2011; 156B(7):751–763. [PubMed: 21858921]
26. Ross CA, Aylward EH, Wild EJ, et al. Huntington disease: natural history, biomarkers and prospects for therapeutics. *Nat Rev Neurol.* 2014; 10(4):204–216. [PubMed: 24614516]
27. Marder K, Zhao H, Myers RH, et al. Rate of functional decline in Huntington's disease. *Huntington Study Group Neurology.* 2000; 54(2):452–458.
28. Tuch DS, Reese TG, Wiegell MR, Makris N, Belliveau JW, Wedeen VJ. High angular resolution diffusion imaging reveals intravoxel white matter fiber heterogeneity. *Magn Reson Med.* 2002; 48(4):577–582. [PubMed: 12353272]
29. Reese TG, Heid O, Weisskoff RM, Wedeen VJ. Reduction of eddy-current-induced distortion in diffusion MRI using a twice-refocused spin echo. *Magn Reson Med.* 2003; 49(1):177–182. [PubMed: 12509835]
30. Han X, Jovicich J, Salat D, et al. Reliability of MRI-derived measurements of human cerebral cortical thickness: the effects of field strength, scanner upgrade and manufacturer. *Neuroimage.* 2006; 32(1):180–194. [PubMed: 16651008]
31. Crawford HE, Hobbs NZ, Keogh R, et al. Corpus callosal atrophy in premanifest and early Huntington's disease. *J Huntingtons Dis.* 2013; 2(4):517–526. [PubMed: 25062736]
32. Majid DS, Aron AR, Thompson W, et al. Basal ganglia atrophy in prodromal Huntington's disease is detectable over one year using automated segmentation. *Mov Disord.* 2011; 26(14):2544–2551. [PubMed: 21932302]
33. Sakaie KE, Lowe MJ. Quantitative assessment of motion correction for high angular resolution diffusion imaging. *Magn Reson Imaging.* 2010; 28(2):290–296. [PubMed: 19695824]
34. Lowe MJ, Beall EB, Sakaie KE, et al. Resting state sensorimotor functional connectivity in multiple sclerosis inversely correlates with transcallosal motor pathway transverse diffusivity. *Hum Brain Mapp.* 2008; 29(7):818–827. [PubMed: 18438889]
35. Smith SM, Jenkinson M, Johansen-Berg H, et al. Tract-based spatial statistics: voxelwise analysis of multi-subject diffusion data. *Neuroimage.* 2006; 31(4):1487–1505. [PubMed: 16624579]
36. Mori S, Oishi K, Jiang H, et al. Stereotaxic white matter atlas based on diffusion tensor imaging in an ICBM template. *Neuroimage.* 2008; 40(2):570–582. [PubMed: 18255316]
37. Bates D, Maechler M, Bolker B, Walker S. Fitting Linear Mixed-Effects Models Using lme4. *Journal of Statistical Software.* 2015; 67(1):1–48.
38. Song SK, Yoshino J, Le TQ, et al. Demyelination increases radial diffusivity in corpus callosum of mouse brain. *Neuroimage.* 2005; 26(1):132–140. [PubMed: 15862213]
39. Gomez-Tortosa E, MacDonald ME, Friend JC, et al. Quantitative neuropathological changes in presymptomatic Huntington's disease. *Ann Neurol.* 2001; 49(1):29–34. [PubMed: 11198293]
40. Song SK, Sun SW, Ju WK, Lin SJ, Cross AH, Neufeld AH. Diffusion tensor imaging detects and differentiates axon and myelin degeneration in mouse optic nerve after retinal ischemia. *Neuroimage.* 2003; 20(3):1714–1722. [PubMed: 14642481]

41. Paulsen JS, Nopoulos PC, Aylward E, et al. Striatal and white matter predictors of estimated diagnosis for Huntington disease. *Brain Res Bull.* 2010; 82(3–4):201–207. [PubMed: 20385209]
42. Delmaire C, Dumas EM, Sharman MA, et al. The structural correlates of functional deficits in early huntington's disease. *Hum Brain Mapp.* 2013; 34(9):2141–2153. [PubMed: 22438242]
43. McColgan P, Seunarine KK, Razi A, et al. Selective vulnerability of Rich Club brain regions is an organizational principle of structural connectivity loss in Huntington's disease. *Brain.* 2015; 138(Pt 11):3327–3344. [PubMed: 26384928]
44. Hobbs NZ, Farmer RE, Rees EM, et al. Short-interval observational data to inform clinical trial design in Huntington's disease. *J Neurol Neurosurg Psychiatry.* 2015; 86(12):1291–1298. [PubMed: 25669748]
45. Catani M, Howard RJ, Pajevic S, Jones DK. Virtual in vivo interactive dissection of white matter fasciculi in the human brain. *Neuroimage.* 2002; 17(1):77–94. [PubMed: 12482069]
46. Rizzolatti G, Cattaneo L, Fabbri-Destro M, Rozzi S. Cortical mechanisms underlying the organization of goal-directed actions and mirror neuron-based action understanding. *Physiol Rev.* 2014; 94(2):655–706. [PubMed: 24692357]
47. Georgiou-Karistianis N, Long JD, Lourens SG, Stout JC, Mills JA, Paulsen JS. Movement sequencing in Huntington disease. *World J Biol Psychiatry.* 2014; 15(6):459–471. [PubMed: 24678867]
48. Say MJ, Jones R, Scahill RI, et al. Visuomotor integration deficits precede clinical onset in Huntington's disease. *Neuropsychologia.* 2011; 49(2):264–270. [PubMed: 21094653]
49. Beaulieu V, Tremblay S, Theoret H. Interhemispheric control of unilateral movement. *Neural Plast.* 2012; 2012:627816. [PubMed: 23304559]
50. Gregory S, Cole JH, Farmer RE, et al. Longitudinal Diffusion Tensor Imaging Shows Progressive Changes in White Matter in Huntington's Disease. *J Huntingtons Dis.* 2015; 4(4):333–346. [PubMed: 26756590]
51. Odish OF, Caeyenberghs K, Hosseini H, van den Bogaard SJ, Roos RA, Leemans A. Dynamics of the connectome in Huntington's disease: A longitudinal diffusion MRI study. *Neuroimage Clin.* 2015; 9:32–43. [PubMed: 26288754]

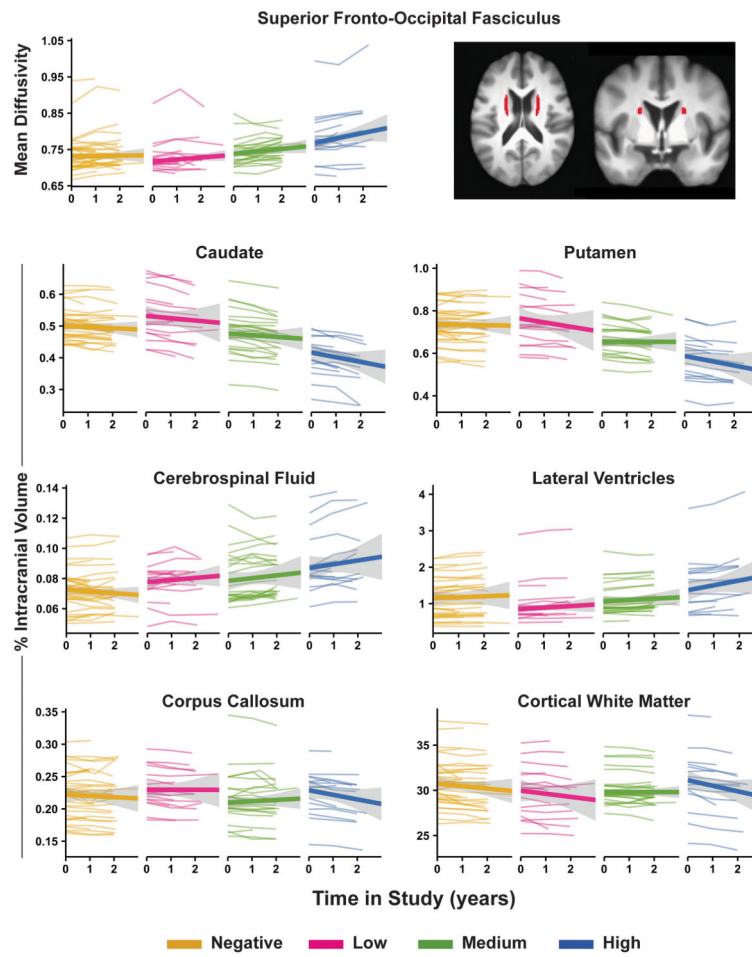


Figure 1. Longitudinal change in MRI variables in gene-negative and positive individuals. Graphs display individual trajectories of longitudinal change for each variable that showed a group by time interaction (Table 3). Variability of individual trajectories (gray) around the group mean trajectory (wide colored line) is shown for each group. The superior-fronto-occipital fasciculus tract is displayed (top right) in axial ($z=18.5$) and coronal ($y=2.5$) views.³⁶

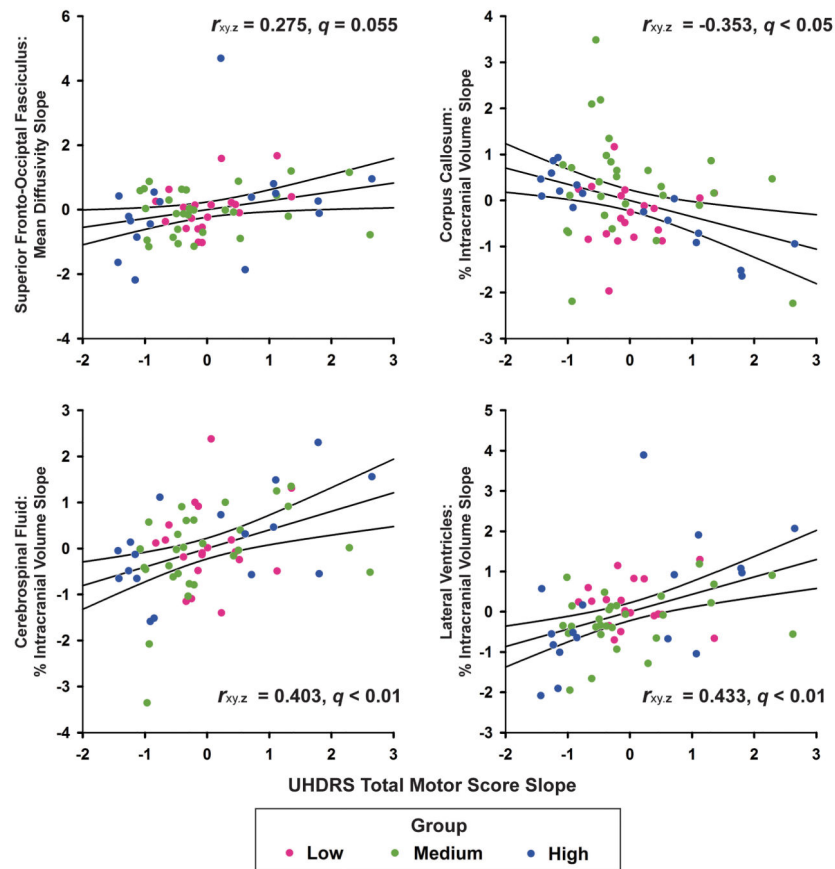


Figure 2.

Association between annualized linear change in MRI variables and linear change in the Unified Huntington's Disease Rating Scale (UHDRS) in gene-positive individuals. Standardized residuals (adjusted for age, CAP, and the number of years between the baseline and final MRI visits) are plotted for the linear slopes of MRI variables that correlated with the slope for the UHDRS total motor score (partial correlations and q-values displayed). Solid lines show the best-fitting linear regression line and 95% confidence intervals. Colored dots designate participants in each prHD group.

Table 1

Demographic, clinical and cognitive variables at baseline visit

	Negative n = 37	Low n = 16	Medium n = 28	High n = 17	Statistic^a	Omega²	Post hoc test^b
Demographic and Clinical							
Age (years)	49.74 (10.09)	32.04 (8.37)	40.86 (10.65)	46.06 (10.93)	13.86 ^{***}	0.28	Low < Neg, Med, High; Med < Neg
Education (years)	15.649 (1.93)	14.79 (2.39)	14.89 (2.42)	14.24 (2.86)	1.63	0.02	
Sex (%female)	68	84	71	82	2.55	-	
CAG repeats	20.162 (3.72)	41.84 (1.74)	42.36 (2.61)	43.77 (3.05)	431.70 ^{***}	0.93	Neg < Low, Med, High
CAP score	-	250.24 (30.73)	330.42 (23.63)	437.35 (42.35)	1568.00 ^{***}	0.98	Low < Med, High; Med < High
Site (Cleveland, Iowa)	15.22	9.10	15.13	9.8	1.33	-	
Unified Huntington's Disease Rating Scale							
Total motor score	4.19 (2.78)	3.32 (2.79)	6.79 (6.42)	11.53 (7.46)	8.89 ^{***}	0.18	High > Neg, Low, Med
Chorea	0.39 (0.80)	0.42 (0.84)	1.18 (2.13)	3.19 (3.54)	7.61 ^{***}	0.16	High > Neg, Low, Med
Oculomotor	1.11 (1.53)	0.84 (1.21)	2.36 (2.20)	2.69 (2.18)	5.10 ^{**}	0.11	High > Neg, Low
Bradykinesia	2.03 (1.81)	1.42 (1.26)	2.89 (2.99)	4.14 (2.90)	3.44 [*]	0.06	High > Neg
Rigidity	0.64 (1.05)	0.47 (0.84)	0.36 (0.87)	0.56 (0.73)	0.57	0.00	
Dystonia	0 (0)	0.16 (0.50)	0 (0)	0.14 (0.34)	-	-	
Cognitive and Sensory Tests							
Stroop Word	107.56 (17.17)	107.37 (12.65)	99.79 (17)	84.59 (22.22)	6.23 ^{***}	0.11	High < Neg, Low
Stroop Color	85.00 (12.01)	84 (10.16)	81 (12.53)	73.77 (16.11)	2.21	0.03	
Stroop Interference	48.36 (10.58)	51.53 (12.78)	49.32 (12.31)	41.29 (12.40)	1.74	0.02	
Symbol Digit Modalities Test	54.39 (10.34)	56.90 (8.58)	54.11 (11.01)	49.71 (9.64)	0.68	0.00	
Trails Part A	22.42 (6.52)	21.47 (7.31)	22.43 (8.06)	28.47 (11.75)	1.94	0.03	
Trails Part B	53.27 (19.13)	47.16 (15.42)	54.41 (23.44)	73.75 (35.85)	2.98 [*]	0.05	High > Neg
UPFIT	0.86 (0.12)	0.87 (0.16)	0.88 (0.08)	0.81 (0.17)	0.92	0.00	

Author Manuscript

Author Manuscript

Author Manuscript

Author Manuscript

F and chi-square (sex, site) statistics. Group differences in cognitive/sensory variables tested using ANCOVA (covarying age and education). No statistical tests were conducted for dystonia due to absence of symptoms in some groups.

* $p < 0.05$,

** $p < 0.01$,

*** $p < 0.001$

q Tukey's honestly significant difference tests

Table 2

Baseline mean (standard error) estimates for imaging and behavioral variables that showed a group effect.

	Negative	Low	Medium	High	Chi-square ^a	Rank ^b
Fractional Anisotropy (FA)						
ALIC	0.410 (0.004)	0.398 (0.005)	0.399 (0.003)	0.394 (0.004)	13.89**	54
BCC	0.575 (0.007)	0.546 (0.009)	0.542 (0.006)	0.535 (0.008)	28.78***	12
CGC	0.456 (0.006)	0.438 (0.008)	0.437 (0.006)	0.425 (0.007)	18.05***	34
CGH	0.236 (0.005)	0.224 (0.006)	0.219 (0.004)	0.228 (0.005)	11.63**	60
EC	0.325 (0.004)	0.315 (0.004)	0.320 (0.003)	0.308 (0.004)	15.59**	43
FS	0.424 (0.006)	0.404 (0.007)	0.412 (0.005)	0.397 (0.006)	18.05***	35
GCC	0.486 (0.007)	0.466 (0.008)	0.462 (0.006)	0.458 (0.007)	17.13***	40
PLIC	0.557 (0.004)	0.547 (0.005)	0.547 (0.004)	0.536 (0.005)	16.29***	41
SCC	0.624 (0.007)	0.601 (0.008)	0.601 (0.006)	0.590 (0.007)	20.86***	27
SCR	0.441 (0.005)	0.424 (0.006)	0.427 (0.004)	0.419 (0.005)	19.41***	30
SFOF	0.437 (0.007)	0.415 (0.009)	0.420 (0.006)	0.403 (0.008)	16.27***	42
Mean Diffusivity (MD)						
ACR	0.802 (0.010)	0.807 (0.013)	0.826 (0.010)	0.847 (0.012)	14.99**	48
ALIC	0.564 (0.004)	0.569 (0.005)	0.573 (0.004)	0.589 (0.005)	24.83***	20
BCC	0.952 (0.011)	0.974 (0.014)	1.000 (0.011)	1.000 (0.013)	19.2***	32
CGC	0.758 (0.005)	0.765 (0.006)	0.767 (0.005)	0.784 (0.006)	17.33***	39
CGH	0.647 (0.009)	0.675 (0.011)	0.683 (0.008)	0.703 (0.010)	29.65***	11
CP	0.347 (0.003)	0.355 (0.004)	0.360 (0.003)	0.366 (0.004)	26.48***	19
EC	0.659 (0.005)	0.668 (0.006)	0.676 (0.005)	0.705 (0.006)	54.27***	2
FS	0.962 (0.014)	1.004 (0.017)	1.006 (0.013)	1.064 (0.016)	35.76***	6
PCR	0.807 (0.010)	0.821 (0.012)	0.844 (0.009)	0.854 (0.011)	19.8***	28
PLIC	0.694 (0.004)	0.699 (0.005)	0.702 (0.003)	0.709 (0.004)	11.67**	59

	<u>Negative</u>	<u>Low</u>	<u>Medium</u>	<u>High</u>	<u>Chi-square^d</u>	<u>Rank^b</u>
PTR	0.897 (0.012)	0.908 (0.015)	0.944 (0.011)	0.976 (0.014)	33.75 ***	9
RLJC	0.800 (0.008)	0.813 (0.01)	0.821 (0.007)	0.840 (0.009)	17.83 ***	37
SCC	0.781 (0.010)	0.799 (0.013)	0.807 (0.010)	0.830 (0.012)	15.5 **	44
SCR	0.730 (0.007)	0.734 (0.009)	0.746 (0.006)	0.756 (0.008)	11.19 *	62
SFOF	0.720 (0.011)	0.740 (0.014)	0.743 (0.010)	0.766 (0.013)	11.31 *	61
SLF	0.738 (0.007)	0.738 (0.008)	0.752 (0.006)	0.767 (0.008)	15.28 **	46
SS	0.900 (0.010)	0.890 (0.012)	0.924 (0.009)	0.948 (0.011)	23.94 ***	22
UNC	0.751 (0.006)	0.754 (0.008)	0.764 (0.006)	0.776 (0.007)	11.8 **	58
Radial Diffusivity (RD)						
ACR	0.615 (0.011)	0.628 (0.014)	0.640 (0.010)	0.666 (0.012)	14.82 **	50
ALJC	0.377 (0.004)	0.386 (0.005)	0.389 (0.004)	0.404 (0.005)	27.06 ***	14
BCC	0.608 (0.012)	0.646 (0.015)	0.668 (0.011)	0.674 (0.014)	28.73 ***	13
CGC	0.545 (0.006)	0.561 (0.008)	0.563 (0.006)	0.585 (0.007)	24.82 ***	21
CGH	0.532 (0.010)	0.562 (0.012)	0.572 (0.009)	0.586 (0.011)	26.54 ***	18
CP	0.212 (0.003)	0.220 (0.004)	0.222 (0.003)	0.231 (0.004)	23.65 ***	23
EC	0.511 (0.005)	0.523 (0.007)	0.528 (0.005)	0.558 (0.006)	51.31 ***	3
FS	0.729 (0.014)	0.775 (0.017)	0.773 (0.013)	0.833 (0.015)	38.46 ***	5
GCC	0.903 (0.021)	0.943 (0.027)	0.951 (0.020)	0.986 (0.024)	10.85 *	63
PCR	0.614 (0.010)	0.628 (0.012)	0.648 (0.009)	0.659 (0.011)	17.97 ***	36
PLJC	0.440 (0.004)	0.448 (0.005)	0.450 (0.004)	0.462 (0.005)	17.8 ***	38
PTR	0.605 (0.012)	0.625 (0.015)	0.650 (0.011)	0.677 (0.014)	26.81 ***	16
RLJC	0.544 (0.008)	0.560 (0.010)	0.562 (0.007)	0.580 (0.009)	14.05 **	53
SCC	0.439 (0.011)	0.468 (0.013)	0.472 (0.010)	0.495 (0.012)	20.99 ***	26
SCR	0.544 (0.007)	0.556 (0.009)	0.562 (0.006)	0.575 (0.008)	14.32 **	52
SFOF	0.536 (0.012)	0.564 (0.015)	0.562 (0.011)	0.591 (0.013)	14.86 **	49
SLF	0.554 (0.007)	0.557 (0.009)	0.567 (0.007)	0.588 (0.008)	15.34 **	45

	<u>Negative</u>	<u>Low</u>	<u>Medium</u>	<u>High</u>	<u>Chi-square^d</u>	<u>Rank^b</u>
SS	0.649 (0.009)	0.646 (0.011)	0.675 (0.008)	0.700 (0.010)	26.71 ***	17
Axial Diffusivity (AD)						
ACR	1.173 (0.011)	1.166 (0.014)	1.198 (0.01)	1.210 (0.013)	11.59 **	60
ALIC	0.939 (0.006)	0.935 (0.008)	0.943 (0.006)	0.958 (0.007)	8.354 *	65
CGH	0.877 (0.010)	0.901 (0.012)	0.904 (0.009)	0.937 (0.011)	27.02 ***	15
CP	0.619 (0.005)	0.626 (0.006)	0.637 (0.005)	0.637 (0.006)	13.26 **	55
EC	0.954 (0.007)	0.957 (0.008)	0.972 (0.006)	0.999 (0.007)	33.97 ***	7
FS	1.428 (0.017)	1.461 (0.021)	1.472 (0.016)	1.529 (0.019)	23.55 ***	24
PCR	1.194 (0.012)	1.207 (0.014)	1.236 (0.011)	1.243 (0.013)	18.32 ***	33
PTR	1.479 (0.015)	1.474 (0.019)	1.530 (0.014)	1.572 (0.017)	33.94 ***	8
RLIC	1.311 (0.012)	1.319 (0.014)	1.339 (0.011)	1.361 (0.013)	14.33 **	51
Brain Volumes						
Caudate	0.497 (0.014)	0.498 (0.018)	0.460 (0.013)	0.396 (0.016)	39.1 ***	4
Putamen	0.757 (0.020)	0.711 (0.024)	0.643 (0.018)	0.579 (0.022)	64.62 ***	1
Pallidum	0.177 (0.007)	0.172 (0.008)	0.156 (0.006)	0.134 (0.007)	32.21 ***	10
Accumbens	0.075 (0.003)	0.073 (0.004)	0.067 (0.003)	0.063 (0.003)	12.9 **	56
CSF	0.071 (0.004)	0.075 (0.004)	0.080 (0.003)	0.087 (0.004)	15.15 **	47
Lat. ventricles	0.932 (0.122)	1.152 (0.152)	1.131 (0.112)	1.365 (0.139)	8.402 *	64
Unified Huntington's Disease Rating Scale						
Total score	4.049 (1.169)	4.093 (1.427)	6.576 (1.067)	10.051 (1.309)	21.2 ***	25
Chorea	0.148 (0.436)	0.358 (0.537)	0.987 (0.401)	2.438 (0.512)	19.38 ***	31
Bradykinesia	2.177 (0.486)	2.308 (0.612)	3.229 (0.455)	4.115 (0.58)	11.98 **	57
Cognitive						
Stroop Word	106.72 (3.843)	109.36 (4.78)	101.33 (3.547)	87.90 (4.362)	19.72 ***	29

^a Chi-square statistics from general linear hypothesis tests for variables showing a significant baseline group effect.

* p<.05;

** p<.01;

*** p<0.001

^b Rank order of baseline group effects based on chi-square statistic. Top 15 variables with the largest chi-square value are in bold font.

ACR = anterior corona radiata; ALIC = anterior limb of internal capsule; BCC = body of corpus callosum; CGC = cingulum-cingulate gyrus; CGH = cingulate gyrus-hippocampus projection; CP = cerebral peduncle; EC = external capsule; FS = fornix and stria terminalis; GCC = genu of corpus callosum; PCR = posterior corona radiata; PLIC = posterior limb of internal capsule; PTR= posterior thalamic radiation; RLIC = retrolenticular part of internal capsule; SCC = splenium of corpus callosum; SCR = superior corona radiata; SFOF = superior fronto-occipital fasciculus; SLF = superior longitudinal fasciculus; SS = sagittal stratum; UNC = uncinata fasciculus; CSF = cerebrospinal fluid; Lat. ventricles = lateral ventricles

Table 3

Linear slope (standard error) estimates for imaging variables that showed a group by time interaction.

	Negative	Low	Medium	High	Chi-square ^a	p value	Rank ^b
Mean Diffusivity							
Superior Frontal Occipital Fasciculus	0.003 (0.002)	0.001 (0.002)	0.006 (0.002)	0.009 (0.002)	9.39	0.0246	6
Brain Volumes							
Caudate	-0.003 (0.002)	-0.006 (0.002)	-0.008 (0.002)	-0.014 (0.002)	23.53	3.14E-05	1
Putamen	-0.002 (0.002)	-0.0033 (0.003)	-0.008 (0.002)	-0.011 (0.002)	17.43	0.0006	2
Corpus callosum	-0.001 (0.001)	-0.003 (0.001)	-0.002 (0.001)	-0.004 (0.001)	15.09	0.0017	4
Cortical white matter	-0.064 (0.052)	-0.157 (0.072)	-0.067 (0.052)	-0.323 (0.066)	14.92	0.0019	5
Cerebrospinal fluid	0.0001(0.001)	0.0005 (0.001)	0.001 (0.001)	0.002 (0.001)	7.82	0.0499	7
Lateral ventricles	0.018 (0.010)	0.031 (0.014)	0.030 (0.010)	0.073 (0.012)	16.55	0.0009	3

^aChi-square statistics from general linear hypothesis tests for variables showing a significant group by time interaction.

^bRank-order of interaction effects based on the chi-square statistic. Higher-ranked variables show a greater annualized rate of change amongst the groups.